Thermal and Electrical Effects of Partial Shade in Monolithic Thin-Film Photovoltaic Modules

Preprint

Timothy J. Silverman, Michael G. Deceglie, Rebekah L. Garris, Chris Deline, and Sarah Kurtz
National Renewable Energy Laboratory

Xingshu Sun and Muhammad Ashraful Alam
Purdue University

This report is available at no cost from the National Renewable Energy
Laboratory (NREL) at www.nrel.gov/publications.

Available electronically at SciTech Connect http:/www.osti.gov/scitech

Available for a processing fee to U.S. Department of Energy
and its contractors, in paper, from:

> U.S. Department of Energy
> Office of Scientific and Technical Information
> P.O. Box 62
> Oak Ridge, TN 37831-0062
> OSTI http://www.osti.gov
> Phone: 865.576.8401
> Fax: 865.576.5728
> Email: reports@osti.gov

Available for sale to the public, in paper, from:

> U.S. Department of Commerce
> National Technical Information Service
> 5301 Shawnee Road
> Alexandria, VA 22312
> NTIS http://www.ntis.gov
> Phone: 800.553.6847 or 703.605.6000
> Fax: 703.605.6900
> Email: orders@ntis.gov

Cover Photos by Dennis Schroeder: (left to right) NREL 26173, NREL 18302, NREL 19758, NREL 29642, NREL 19795.

NREL prints on paper that contains recycled content.

Thermal and electrical effects of partial shade in monolithic thin-film photovoltaic modules

Timothy J Silverman*, Michael G. Deceglie*, Xingshu Sun†, Rebekah L. Garris*,
Muhammad Ashraful Alam†, Chris Deline*, Sarah Kurtz*

*National Renewable Energy Laboratory, Golden, Colorado, 80401, United States
†Purdue Univeristy, West Lafayette, Indiana, 47907, United States

Abstract—**Photovoltaic cells can be damaged by reverse bias stress, which arises during service when a monolithically integrated thin-film module is partially shaded. We introduce a model for describing a module's internal thermal and electrical state, which cannot normally be measured. Using this model and experimental measurements, we present several results with relevance for reliability testing and module engineering: Modules with a small breakdown voltage experience less stress than those with a large breakdown voltage, with some exceptions for modules having light-enhanced reverse breakdown. Masks leaving a small part of the masked cells illuminated can lead to very high temperature and current density compared to masks covering entire cells.**

I. BACKGROUND AND INTRODUCTION

Photovoltaic (PV) cells can be damaged by reverse bias stress. This can occur in service when a module is partially shaded, as illustrated in Fig. 1. The large number of cells in the module can provide the driving force for reverse breakdown to occur and this can in turn lead to high temperature, high current density and high reverse voltage. At the module scale it is not generally possible to observe a specimen's complete internal electrical and thermal state. This information is of great interest for linking specific stress conditions or manufacturing defects to performance and reliability problems.

High temperature drives thermally-activated failures such as the degradation or delamination of packaging. Localized defects may result in locally much higher temperature, which

Fig. 1. Cropped electroluminescence image of a commercial CIGS module. The dark areas indicate widespread shunting in an area that was covered with an opaque mask while the module was briefly exposed to light. The cell pitch is approximately 5 mm.

can lead to problematic physical or chemical changes in the semiconductor device itself. Current density is the driving force for degradation due to electromigration [1] and, in reverse bias, accompanies the dissipation of power as heat. High voltage between the contacts drives the diffusion of charged species and possibly "lightning rod" effects near asperities in the metal contact. When shunts are present, high voltage can also drive large currents through these shunts, resulting in locally very high temperature. Because these effects emerge as a consequence of the large-scale interconnection of a module, it is not obvious what stress may result from a given combination of junction characteristics and module illumination pattern. Nonuniformities in the module itself may also interact with illumination nonuniformity, changing the resulting stress.

To address the need to predict the internal electrical and thermal stress in a module under arbitrary patterns of illumination, we developed a model of a monolithic PV module that couples a two-dimensional electrical model with a three-dimensional model of heat transfer in the module package. The model improves in various ways upon existing isothermal module-scale electrical-only models and those coupled to two-dimensional heat transfer models [2], [3], [4].

The reverse breakdown of copper indium gallium diselenide (CIGS) has been found to depend on illumination [5], [6], [7]. The reverse breakdown voltage of some CIGS cells is much smaller under illumination than in darkness. The physical origin of this light-enhanced reverse breakdown (LERB) effect, which is different from illumination-dependent shunt current, is still an active area of research. Modules with LERB would violate assumption in existing module-scale models of a light-independent reverse *JV* curve and would introduce a strong dependence of internal stress on the irradiance incident on masked cells. Our work includes the effects of LERB for the first time in a module-scale simulation. We explore the consequences of LERB, mask size and mask transmissivity in partial shade simulations at the module scale and consider their relevance for reliability testing.

II. METHOD

A. Cell measurements

LERB has previously been observed in laboratory-scale cells and in cells deposited on polymer substrates, which may not be representative of mainstream monolithically integrated
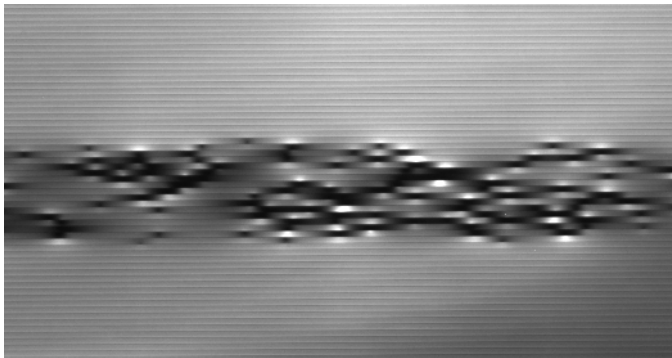
CIGS modules [5], [6], [7]. To establish the relevance of this phenomenon to commercial products, we measured the *JV* curve of a single ~5 cm^2 cell in a coupon cut from an unencapsulated commercial monolithically integrated CIGS module. The measurement was performed in a class AAA solar simulator at 1,000 Wm^{-2}, at 100 Wm^{-2} using a mask with ~10% transmissivity, and in darkness.

B. Module-scale simulations

We simulated the steady-state coupled heat transfer and electrical continuity problem of an operating monolithic thin-film PV module using commercial finite element analysis software, COMSOL Multiphysics. The finite element approach enabled the model to be nonuniformly discretized so that microscopic details could be simulated without the computational expense of simulating the entire module at the microscopic scale.

The front and back contacts of each cell in the module were simulated two-dimensionally in the plane of the module. The steady-state voltage V in the contacts is governed by the conservation of current, $\nabla \cdot (-\sigma \nabla V) = Q_j$ where Q_j is a current source and σ is electrical conductivity. The term in parentheses is current density. The cell itself was treated one-dimensionally with a compact model simulating its IV curve. More detail about the compact model is presented in Section II-C. The top and bottom contacts were electrically connected to one another according to the cell model. This was achieved with a current sink in one contact and corresponding source in the other. Although we assumed uniform junction behavior in this work, the model supports arbitrary patterns of nonuniformity. The interconnect area between cells was modeled as a segment of back contact in series with a segment of front contact. The first and last cell boundaries could be set to a fixed voltage or adjusted to pass a fixed current density.

We simulated the steady-state heat transfer by conduction in the module package in three dimensions. The temperature T in the module package is governed by the conservation of energy, $\nabla \cdot (-k \nabla T) = Q$ where Q is a heat source and k is thermal conductivity. The term in parentheses is heat flux. Heat absorbed and dissipated by the photovoltaic device was introduced to the package as a two-dimensional heat source at the device plane. The outer surfaces of the module package were subject to a convection heat transfer boundary condition, $-k \nabla T = h (T_\infty - T)$, where h is a convection heat transfer coefficient and T_∞ is the ambient temperature. Radiation heat transfer and the conversion in the packaging materials of solar radiation to heat were neglected.

In this work, we considered monolithic CIGS modules. CIGS is typically deposited in a substrate configuration, so the front contact is a transparent conductive oxide (TCO) and the rear contact is metallic. The device plane is at the rear side of the ethylene-vinyl acetate (EVA) encapsulant in a glass-encapsulant-glass package. The parameters used for this module-level model are summarized in Table I.

We investigated the thermal and electrical consequences of partial shade in a 20-cell, 100 cm^2 (0.1 m × 0.1 m)

TABLE I
PARAMETER VALUES USED IN THE MODULE-LEVEL MODEL.

glass thermal conductivity	1.1 Wm^{-1}K^{-1}
glass thickness	3.2 mm
EVA thermal conductivity	0.311 Wm^{-1}K^{-1}
EVA thickness	0.5 mm
metal contact sheet resistance	1 Ω/□
oxide contact sheet resistance	10 Ω/□
ambient temperature	25°C
convection heat transfer coefficient	20 Wm^{-2}K^{-1}
cell pitch	5 mm
cell dead area	300 μm
metal interconnect effective length	230 μm
oxide interconnect effective length	2 μm

mini-module and in a 100-cell, 2,500 cm^2 (0.5 m × 0.5 m) module. We first simulated a quasi-steady-state *IV* curve at uniform illumination of 1,000 Wm^{-2} so as to identify the module-level maximum power current (I_{mp}) at the module's steady-state operating temperature. All subsequent simulations were performed with the module passing this unshaded I_{mp}, simulating the module's integration in a long series string of similar, unshaded modules.

Using each of the three reverse characteristics discussed in Section II-C we simulated multiple partial shade scenarios wherein portions of a module otherwise uniformly illuminated at 1,000 Wm^{-2} were covered with a mask. In the 20-cell mini-module geometry, we simulated the application of masks covering two cells in the center of the module. In the 100-cell module, we simulated the application of masks covering eight cells in the center of the module. The masks ranged in transmissivity from 0.0 to 1.0 and in size from covering 0% to 100% of the long dimension of the masked cells.

Commercial CIGS modules often contain microscopic shunts. To establish the suitability of our modeling approach for simulating interactions between illumination nonuniformity and these microscopic defects, we simulated a 50 cm^2 (0.1 m × 0.05 m) mini-module composed of ten series-connected cells with a 5 μm radius circular shunt randomly placed in each cell. The shunts provided a very low-resistance current path between the top and bottom contacts. We simulated the module's steady-state response to uniform illumination under short-circuit conditions. This model was discretized to show the temperature, voltage and current distribution in very fine detail surrounding the defects.

C. Compact model characteristics

The local *JV* characteristic in the module-level model was simulated with a physics-based compact model, obtained by integrating the photo-induced electron and hole transport equations across the absorber layer [8]. In forward bias, this model described the CIGS cell as a heterojunction device with bias-dependent carrier collection. The reverse-breakdown behavior was modeled phenomenologically as tunneling-assisted Poole-Frenkel transport. This enabled the description of LERB as a light-induced change in the dominant defect level associated with the reverse current. We selected Poole-Frenkel transport

to model the reverse-breakdown effect because, unlike Zener and avalanche breakdown, it is consistent with the doping level of CIGS/CdS and with the observed temperature dependence of reverse breakdown in CIGS [6], [9]. Avalanche breakdown has a the opposite temperature coefficient from the observed one and, given the typical doping of CdS and CIGS, avalanche breakdown voltage is expected to be approximately 10 V, which is much larger than the observed values. Zener breakdown has a very weak dependence on temperature and the breakdown voltage that would be expected based on the typical doping level, approximately 2 V, is smaller than the observed values. The compact model is summarized in Table II and more detail is available in our related paper [8].
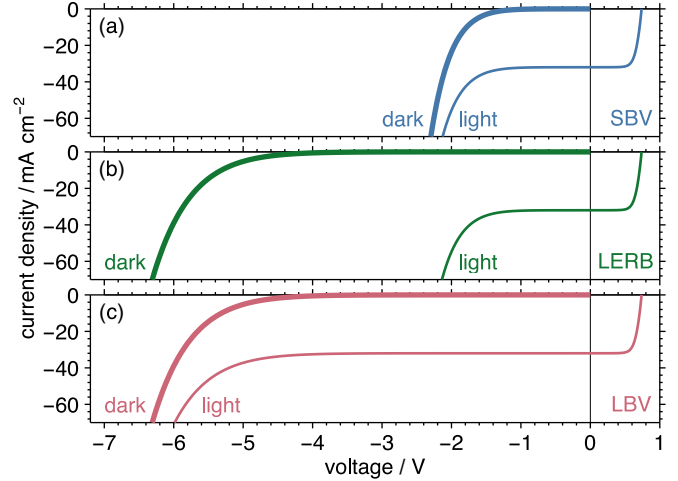

Fig. 2. The dark (heavy lines) and light (light lines) *JV* curves for the three different characteristics used in the module-scale model. The small breakdown voltage (SBV) characteristic (a) had a small, illumination-independent breakdown voltage. The light-enhanced reverse-breakdown (LERB) characteristic (b) had a smaller breakdown voltage under illumination than in darkness. The large breakdown voltage (LBV) characteristic (c) had a large, illumination-independent breakdown voltage.

TABLE II
SUMMARY OF THE COMPACT DEVICE MODEL.

$$J_{\text{photo}} = J_{\text{total}} \frac{1 - \exp\left(-\Delta\sqrt{\frac{V_{\text{bi}}-V}{V_{\text{bi}}}}\right)}{1 + \alpha_c \exp\left(\beta\frac{q(V-V_{\text{bi}})}{kT}\right)}$$

$$J_{\text{RB}} = J_{0,\text{RB}} V \exp\left(\frac{q}{kT}\sqrt{\frac{V}{m}}\right)$$

$$J_{\text{shunt}} = G_{\text{sh}}V + I_{0,\text{sh}}V^{n_{\text{sh}}}$$

$$J_{\text{diode}} = J_0\left[\exp\left(\frac{qV}{nkT}\right) - 1\right]$$

J_{total}	total generation current density
Δ	product of equilibrium depletion width and average absorption coefficient
V_{bi}	junction built-in potential
α_c	ratio between front and back surface recombination velocities
β	voltage partition factor
$J_{0,\text{RB}}$	breakdown current density prefactor (function of illumination intensity)
m	breakdown current index
G_{sh}	ohmic shunt conductance
$I_{0,\text{sh}}$	space charge limited shunt conductance
n_{sh}	shunt current ideality factor
J_0	diode saturation current density
n	diode ideality factor

To explore the effect of LERB on the stress resulting from partial shade, we simulated three different local *JV* characteristics, illustrated in Fig. 2. The small breakdown voltage (SBV) reverse characteristic was illumination-independent and matched the reduced breakdown voltage of the fully-illuminated LERB characteristic. The large breakdown voltage (LBV) characteristic was also illumination-independent but matched the large breakdown voltage of the LERB characteristic in total darkness. For clarity, only the room-temperature dark and light *JV* curves are shown in the figure; simulations were carried out using the complete temperature- and irradiance-dependent *JV* characteristics.

D. Module testing

To qualitatively validate the simulation results, we performed an indoor partial shade stress test on a full-size commercial monolithically integrated CIGS module with between 100 and 200 series-connected cells. We applied a mask with 10% transmissivity to ten cells near the center of the module. The mask covered 50% of the long dimension of these cells. We placed the module in a class BBA continuous solar simulator at 1,000 Wm^{-2} irradiance. The module was placed at open circuit while it warmed up for ten minutes, then stressed at I_{mp} for ten minutes. During the stress, we collected maps of the back surface temperature of the module using an infrared (IR) thermography camera with a 1280 pixel × 720 pixel resolution InSb detector.

III. RESULTS AND DISCUSSION

A. Cell measurements

JV curves from the commercial coupon are shown in Fig. 3. The curves are shifted upward by j_{sc} so that they all pass through the origin, aiding in comparison of the reverse-bias behavior. The reverse-bias behavior shows a clear dependence on illumination. These measurements were made repeatedly and resulted in no appreciable permanent change in the cell. Based on this observation of LERB in a commercial CIGS product, we note the importance of determining the effects of LERB on the stress resulting from partial shade of commercial modules.

B. Module-scale simulations

Using results from simulations of the mini-module geometry, we show in Fig. 4 the peak temperature, current density and reverse voltage as a function of mask extent and transmissivity. The left column shows results for the mask covering 90% of the long dimension of the masked cells, as illustrated in the inset of Fig. 4(a). The right column shows
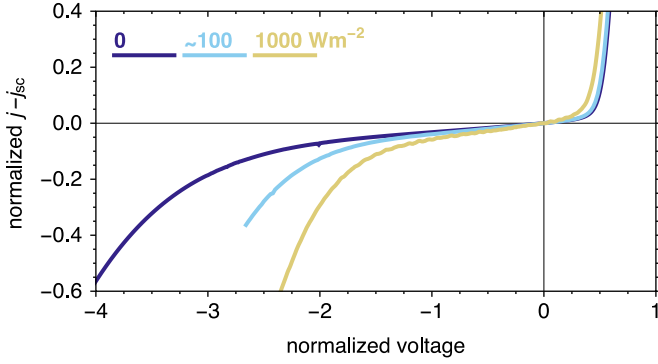
Fig. 3. *JV* curves measured on a single $\sim$5 cm^2 cell in a coupon cut from an unencapsulated commercial monolithically integrated CIGS module. Each curve has been shifted by j_{sc} so as to pass through the origin. The reverse-bias behavior of the sample has a clear dependence on illumination. Current density and voltage are normalized to j_{sc} and V_{oc}, respectively, under 1,000 Wm^{-2}.

results for the mask completely covering the masked cells, as shown in the inset of Fig. 4(b).

In every condition, the module with the SBV characteristic showed equal or lower stress compared to the ones with the LERB and LBV characteristics. This suggests that a small reverse breakdown voltage is desirable for partial shade durability, as long as the breakdown itself does not result in damage. Smaller breakdown voltage is also desirable from a performance perspective because the module will continue producing power with a larger number of cells shaded.

In most conditions, stress in the module with the LBV characteristic exceeds that in the other two modules. This results from the module's electrical boundary condition, which requires that a total of I_{mp} must flow through each cell of the module regardless of its illumination state. In the modules with masks covering 100% of the area of the masked cells, the current density is thus nearly independent of mask transmissivity and of junction characteristic (Fig. 4(d)). This means that, with a larger breakdown voltage, a higher density of power is dissipated in the masked cells, resulting in higher peak temperature for the LBV module (Fig. 4(b)).

In modules with masks covering 90% of the area of the masked cells, the peak current density and temperature are governed by the fact that current flows preferentially in the unmasked area of the masked cells. This is illustrated in Fig. 5, which shows the lateral current density in the back contact of the unshaded portions of cells that are 90% covered in the 100-cell module geometry. Huge lateral current densities develop to route the current from the uniformly illuminated cells through the illuminated portion of the masked cells. Because current can only reach an adjacent cell's back contact by first passing through the junction, this phenomenon is accompanied by very large junction current density in the unmasked portions of masked cells. This is illustrated in Fig. 4(c) and the resulting high peak temperature is visible in Fig. 4(a).

In the LERB module, current density and temperature exceed those reached in the LBV module only in the limit of
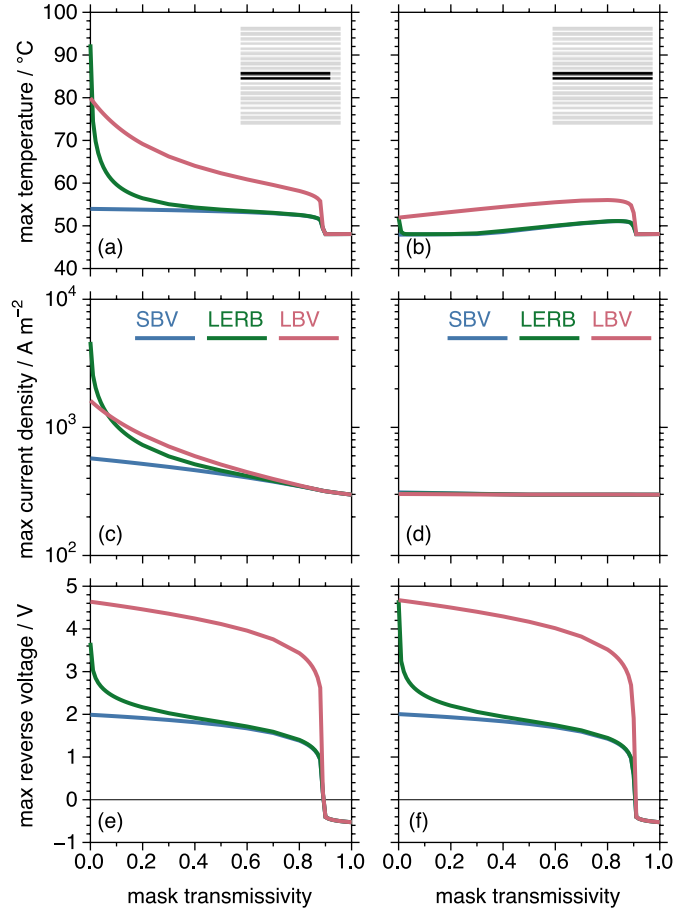

Fig. 4. The simulated steady-state peak value of three stresses (temperature, junction current density and voltage) are shown as functions of device characteristic and mask extent and transmissivity. The simulation results are for a 20-cell, 100-cm^2 mini-module. Results for masks covering 90% (left column) and 100% (right column) of the module width are shown for the three characteristics introduced in Fig. 2. The 90% mask width causes equal or greater stress than the 100% mask width in nearly every case. The junction current density and temperature stresses in the LERB module become very large as the mask approaches zero transmission. The SBV characteristic has the lowest stress in every case.

low-transmissivity (nearly opaque) masks that cover 90% of the cells (Fig. 4(a) and Fig. 4(c)). Under these conditions, the illuminated and masked portions of the masked cells, which are held at nearly the same voltage by the contact layers, pass radically different amounts of current. This is made clear by selecting a moderate reverse voltage in Fig. 2(b) and observing that the light *JV* curve must pass a much higher current density to reach the same voltage.

In practice it is difficult to block all light to a fraction of the PV cells in a monolithic thin-film module, even intentionally. This is because there is normally $\sim$ 4 mm of transparent packaging between the PV cells and the module's front surface. This suggests that, in cells with LERB, some of the beneficial reduction in breakdown voltage by light may practically always be available. We note, however, that the diversity in CIGS forward-bias behavior implies that there
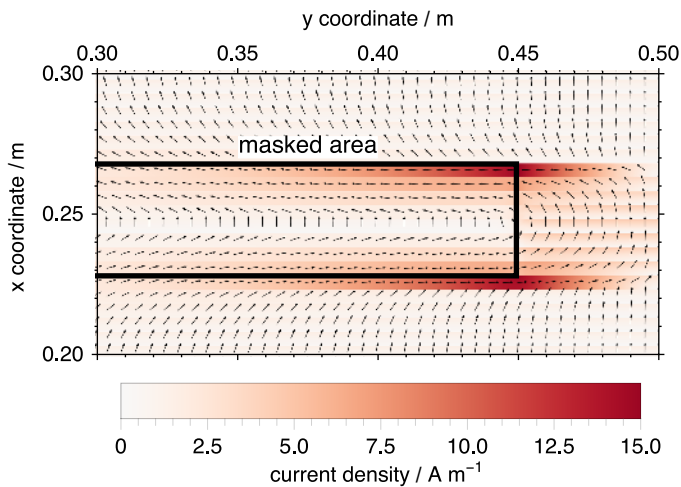
Fig. 5. A lateral current density map showing current in the back contact of part of a 100-cell, 2,500 cm^2 (0.5 m × 0.5 m) module with the LERB characteristic. Current magnitude is indicated with color and direction is indicated with arrows. The area outlined in black is covered in a 10% transmitting mask and the plot shows the only unmasked portion of the masked cells. Most of the current of the completely unmasked cells must pass through this narrow unmasked region in the masked cells, resulting in very high lateral current density (shown here) in addition to very high junction current density and temperature (not shown).
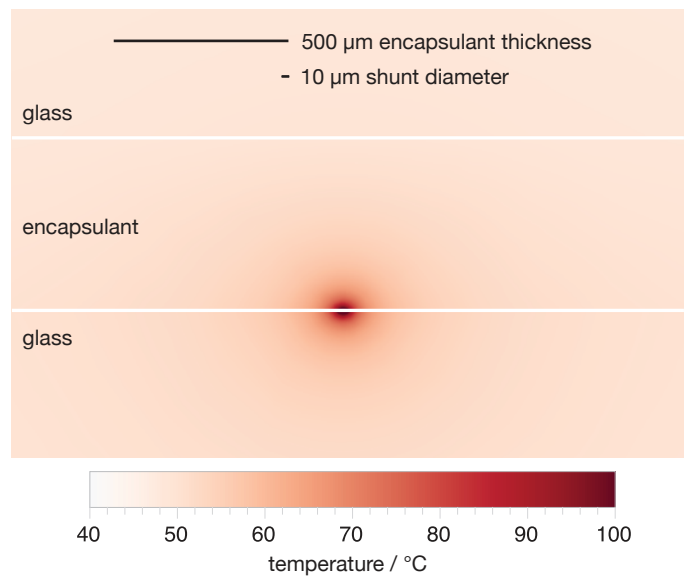

Fig. 6. Simulated cross-sectional temperature map for a microscopic shunt in a mini-module. The temperature distribution illustrates the three-dimensional nature of heat transfer near small defects in the module package. Note that the shunt's peak temperature is 135 °C and the color scale has been adjusted for clarity.

may be an equal diversity in reverse-bias behavior. Although they are for one specific set of cell behaviors, our results are sufficient to show that partial shade stress is sensitive to a module's reverse bias characteristic, including to the dependence of this characteristic on illumination.

As shown in Section III-C, the thermal response of commercial CIGS modules is often influenced by microscopic shunts. Some of these shunts are present when the module is new, but others can form during stress. Our model of a mini-module containing microscopic shunts simulates this important effect. A temperature map through the cross-section of one of the shunts in the shunted mini-module is shown in Fig. 6. This map shows the three layers of the package (front glass, EVA and rear glass) with the elevated temperature due to the shunt shown at the rear surface of the encapsulant. At steady state, the shunt itself reaches 135°C, a temperature sufficient to cause accelerated degradation or delamination of polymer packaging materials. It is clear that the temperature distribution around such a localized feature is three-dimensional, motivating the need for a three-dimensional thermal model to be coupled to two-dimensional electrical models.

C. Module testing

The temperature map resulting from the module partial shade test is shown in Fig. 7(b). The figure shows a cropped view of a larger module. Results from a simulation of the same shade condition on the 100-cell module with LERB is shown in Fig. 7(a). The large scale behavior of the simulation matches the experimental result: the masked area is cooler and the unmasked area of the masked cells is made hotter by the preferential flow of current there. However, on the

small scale the experimental temperature map is dominated by heating from localized shunts, some of which formed during the test. In the temperature map, these shunts appear even in the illuminated portion of the masked cells because the voltage across these portions of the cells is still large enough to cause locally high current flow.
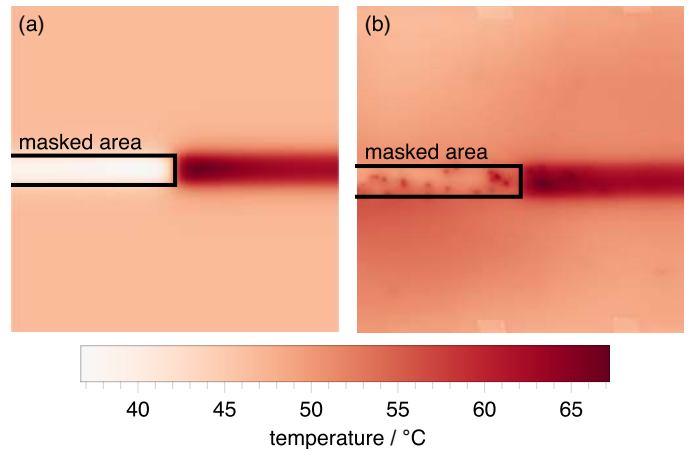

Fig. 7. Simulated (a) and experimental (b) maps of back-of-module temperature for modules with several cells 50% covered by a 10% transmitting mask. In both measurement and simulation, the module was loaded at its unshaded I_{mp}. The masked region is labeled and outlined in black. The simulated map (a) shows the entire area of a 100-cell, 2,500 cm^2 (0.5 m × 0.5 m) module with the LERB characteristic. The experimental map (b) shows a 0.6 m × 0.6 m portion of a larger commercial CIGS module. Heating from localized shunting is visible in both the masked and unmasked areas of the masked cells in the experimental map.

The prominence of localized defects in Fig. 7(b) suggests it

may be important to consider preexisting and emerging defects in determining the internal thermal and electrical response of a module to partial shade stress. The module-scale model we have introduced here can describe these (as in Fig. 6).

IV. CONCLUSION

Partial shade in monolithic thin-film modules can cause reverse bias operation, which leads to temperature, current density and voltage stress. The magnitude of this stress is sensitive to mask transmissivity and extent. Masks that leave portions of the masked cells illuminated lead to higher temperature and current density because of the preferential flow of current through the illuminated portions.

We showed that the previously reported illumination dependence of reverse-bias behavior (LERB) is present in some commercial CIGS cells, with breakdown voltage becoming much smaller under illumination. We incorporated this effect for the first time in a module-scale model, which we used to predict thermal and electrical stress due to partial shade. Provided the breakdown itself does not cause permanent damage, small breakdown voltage results in lower stress in most of the cases we considered. The exceptions were cases of nearly opaque, partial-extent masks, wherein light-enhanced reverse breakdown can cause locally higher temperature and current density compared to modules with light-independent reverse breakdown.

The high sensitivity of stress to the shape and extent of masks and to the details of a module's reverse-bias behavior underscores the need to consider these effects when designing reliability tests and when engineering the thin-film modules themselves.

V. ACKNOWLEDGMENTS

REFERENCES

[1] S. Dongaonkar, K. Yogendra, S. Mahapatra, and M. Alam, "Physics and statistics of non-ohmic shunt conduction and metastability in amorphous silicon p-i-n solar cells," *Photovoltaics, IEEE Journal of*, vol. 1, no. 2, pp. 111–117, Oct 2011.

[2] G. Janssen, L. Slooff, and E. Bende, "2D - finite element model of a CIGS module," in *Photovoltaic Specialists Conference (PVSC), 2012 38th IEEE*, June 2012, pp. 001 481–001 485.

[3] S. Dongaonkar, C. Deline, and M. Alam, "Performance and reliability implications of two-dimensional shading in monolithic thin-film photovoltaic modules," *Photovoltaics, IEEE Journal of*, vol. 3, no. 4, pp. 1367–1375, Oct 2013.

[4] F. W. Fecher, A. P. Romero, C. J. Brabec, and C. Buerhop-Lutz, "Influence of a shunt on the electrical behavior in thin film photovoltaic modules – a 2D finite element simulation study," *Solar Energy*, vol. 105, no. 0, pp. 494 – 504, 2014.

[5] P. Mack, T. Walter, R. Kniese, D. Hariskos, and R. Schäffler, "Reverse bias and reverse currents in CIGS thin film solar cells and modules," in *23rd European Photovoltaic Solar Energy Conference and Exhibition*, 2008.

[6] P. Szaniawski, J. Lindahl, T. Törndahl, U. Zimmermann, and M. Edoff, "Light-enhanced reverse breakdown in Cu(In,Ga)Se2 solar cells," *Thin Solid Films*, vol. 535, no. 0, pp. 326 – 330, 2013.

[7] S. Puttnins, S. Jander, K. Pelz, S. Heinker, F. Daume, A. Rahm, A. Braun, and M. Grundmann, "The influence of front contact and buffer layer properties on CIGSe solar cell breakdown characteristics," in *26th European Photovoltaic Solar Energy Conference and Exhibition*, 2014.

[8] X. Sun, J. Raguse, T. J. Silverman, C. Deline, and M. Alam, "A physics-based compact model for CIGS and CdTe solar cells: from voltage-dependent carrier collection to light-enhanced reverse breakdown," in *42nd IEEE Photovoltaics Specialists Conference (PVSC)*, June 2015.

[9] S. M. Sze and K. K. Ng, *Physics of Semiconductor Devices*. Wiley-Interscience, 2006.